PROCEEDINGS OF SPIE

SPIEDigitalLibrary.org/conference-proceedings-of-spie

Optimization of a SS-OCT with a focus tunable lens for enhanced visualization of ocular opacities

Ana Rodríguez Aramendía, Ireneusz Grulkowski, Alfonso Jiménez Villar, Silvestre Manzanera, Yiwei Chen, et al.

Ana Rodríguez Aramendía, Ireneusz Grulkowski, Alfonso Jiménez Villar, Silvestre Manzanera, Yiwei Chen, Juan Mompean, Fernando Díaz-Doutón, Jaume Pujol, José Luis Güell, Pablo Artal, "Optimization of a SS-OCT with a focus tunable lens for enhanced visualization of ocular opacities ," Proc. SPIE 10867, Optical Coherence Tomography and Coherence Domain Optical Methods in Biomedicine XXIII, 108673E (22 February 2019); doi: 10.1117/12.2508640

SPIE.

Event: SPIE BiOS, 2019, San Francisco, California, United States

Optimization of a SS-OCT with a focus tunable lens for enhanced visualization of ocular opacities

Ana Rodríguez-Aramendía[1,2], Ireneusz Grulkowski[3], Alfonso Jiménez-Villar[3], Silvestre Manzanera[4], Yiwei Chen[4], Juan Mompeán[4], Fernando Díaz-Doutón[2], Jaume Pujol[2], José Luis Güell[1], Pablo Artal[4]

[1]Instituto de Microcirugía Ocular, Barcelona, Spain
[2]Center for Sensors, Instruments and Systems Development, Universitat Politècnica de Catalunya, Barcelona, Spain
[3]Faculty of Physics, Astronomy and Informatics, Nicolaus Copernicus University in Torun, Torun, Poland
[4]Laboratorio de Óptica, Universidad de Murcia, Murcia, Spain

ABSTRACT

Optical methods have been recently used to perform objective assessment of crystalline lens and corneal opacities. Swept-source optical coherence tomography (SS-OCT) enables measurements of the back-reflected or back-scattered photons from the internal objects. In this work, we present a long-depth range SS-OCT system, with a focus tunable lens, optimized for the visualization of large sections of the posterior segment of the eye, including the vitreous. The system was validated using an eye model.

Keywords: ocular opacities, vitreous, optical coherence tomography, swept-source optical coherence tomography, tunable lens

1. INTRODUCTION

Intraocular scattering degrades the contrast in retinal imaging and impairs visual quality[1]. In the clinical practice assessment of opacities is mainly based on the subjective evaluation of slit-lap microscopy images. However several other methods to measure intraocular scattering have been proposed and can be classified into two categories: imaging-based techniques and straylight measurement approaches[2,3]. While some of these methods lack the ability of differentiating the contribution of different ocular structures or are mostly dedicated to lens and corneal opacities, the specific role of vitreous opacities in optical and visual quality has remained scarcely explored[4-8]. One of the reasons for that is that the evaluation *in vivo* of the properties of the vitreous has long been rendered difficult[9,10].

Optical coherence tomography instruments have demonstrated to be a powerful tool in the assessment of crystalline lens and corneal opacities[2,3]. Recent works have shown that swept source – optical coherence tomography (SS-OCT) systems combined with electrically tunable lenses (ETL) also allow enhancing the visualization of the vitreous structures both close to the posterior surface of the lens and to the retina[11-16]. In this paper, we describe a long-depth range SS-OCT instrument with a custom designed sample arm interface using a focus tunable lens specifically designed and optimized to visualize ocular opacifications, with a large volume of the vitreous. The proposed system opens the possibility to study separately opacification processes in the anterior segment structures and the vitreous.

2. METHODS

A high-speed swept-source OCT instrument operating at a central wavelength of 1050 nm for long-range imaging has been developed. The system utilizes a short external cavity tunable laser source with a sweep rate of 50 kA-scans/second and 100 nm tuning range. The sufficiently long coherence length of the source together with a dedicated fast acquisition

Optical Coherence Tomography and Coherence Domain Optical Methods in Biomedicine XXIII
edited by James G. Fujimoto, Joseph A. Izatt, Proc. of SPIE Vol. 10867, 108673E

system allows for a long imaging depth range, fitting the requirements of this application. The system is versatile and permits to interchange easily the patient interface.

We have designed a patient interface specially dedicated to vitreous humor imaging (Fig. 1). The designed interface consists of a collimator, a tunable lens (Optotune, Switzerland), a set of XY galvanometer mirrors and a telescope system and has been optimized by means of optical design simulation software (Zemax, Radiant Zemax LLC). The collimator produces a collimated beam of 3.37 mm diameter. Two custom lenses groups L1 and L2, of effective focal lengths of 80 mm and 40 mm, respectively, form a telescope of magnification 0.5[17] .The pivot of the scanning relays on the pupil plane of the eye. The Liou-Brennan eye model has been utilized in the simulation. In an effort to maximize the size of the vitreous sample probe, 2" diameter lenses have been chosen.

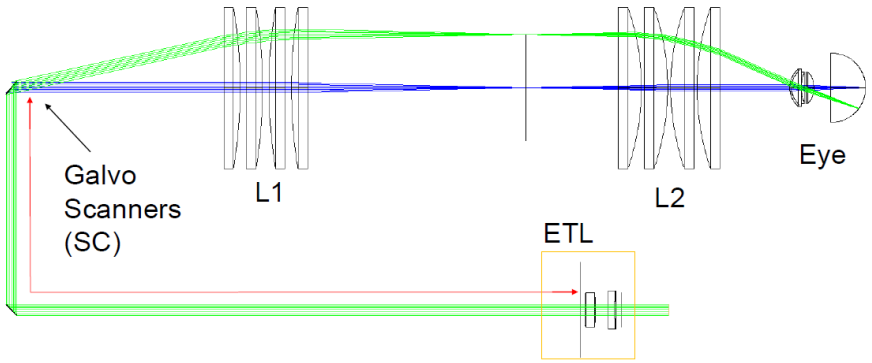

Figure 1. The vitreous imaging interface designed for this work consists in a collimator, an ETL with an offset lens, a XY galvanometer scanners set, and a telescope system formed by two custom lenses groups L1 and L2.

The focus-tunable lens is combined with an integrated offset lens, which is a negative power singlet, to adjust the tunable lens power range appropriately for the application. Model EL-10-30-C-NIR-LD-MV (Optotune) has been chosen for the design (Fig. 2a). The ensemble offers a tunable optical power range from -1.5 diopters to +3.5 diopters, as shown in Fig. 2b.

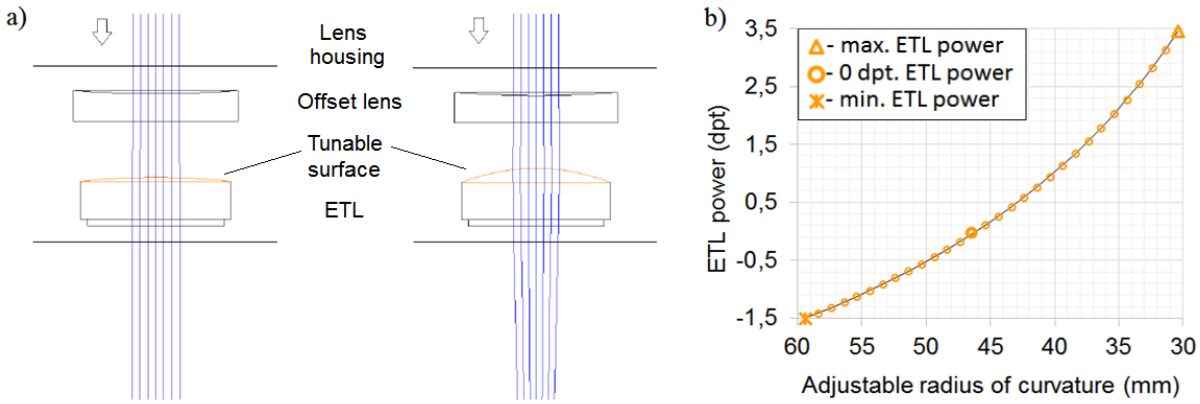

Figure 2. (a) The ensemble ETL and negative power offset lens (EL-10-30-C-NIR-LD-MV (Optotune)) Zemax model for simulation purposes. (b) Optical power of the tunable lens as a function of the radius of curvature of the adjustable surface, which can be tuned in the range from -1.5 to +3.5 diopters.

The interface has been designed so that the focal plane of the system relays on the retina when the ETL power is 0 diopters, with a lateral resolution of about 13 µm and offering a 45º field of view (FOV) in the retina. Increasing the ETL power allows to tune the focal plane towards the posterior face of the lens. The distance from ETL to galvanometric

scanners has been chosen to be 250 mm so as to achieve the desired focus position range with the available ETL power range.

Figure 3a shows the best focus depth for a central field (0º) and the most external field (22.5º). The focal plane shifts away about 10 mm (central field) from the retina for the maximum ETL power. The best focus surface adopts a larger curvature as it approaches the posterior face of lens. The lateral resolution decreases from 13 µm (retina) to about 30 µm (maximum ETL power), as depicted in Fig. 3b.

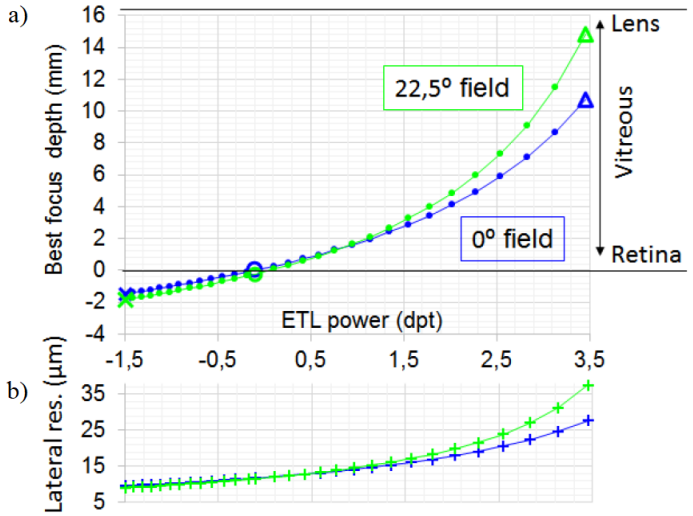

Figure 3. (a) Best focus depth as a function of ETL optical power. (b) Lateral resolution (Airy radius) as a function of ETL optical power.

In Fig. 4, the optical performance of the interface is illustrated. The upper part of the figure shows where the focal plane of the interface lies within the eye model for different ETL powers. A central field (0º, 0º) and an external field (0º, 22.5º) are shown in the simulation in blue and green, respectively. The lower part of the figure features the corresponding spot diagram of both fields for different ETL powers.

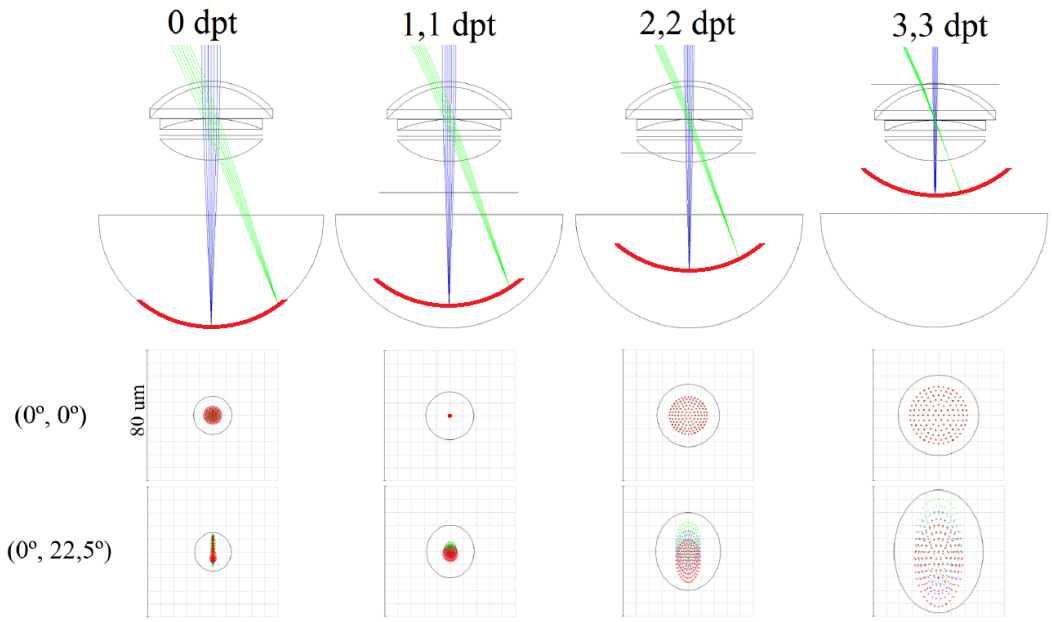

Figure 4. Simulation and spot diagrams for a central (0º, 0º) and an external field (0º, 22.5º) for different ETL powers.

3. RESULTS

According to the above described design, a dedicated sample arm has been incorporated to a laboratory prototype (Fig. 5a). To validate the performance of the system, a custom-made eye model has been used (Fig. 5b-c). It is composed of a biconvex lens of 25.4 mm focal length mounted on a structure with a small container where artificial vitreous gel can be placed in. A movable plate with a printed calibrated target closes the chamber on the other end and features a plastic membrane that acts as a seal to prevent the artificial vitreous to leak out.

The artificial vitreous used in the preliminary tests is mainly composed of water and two different types of water soluble synthetic polymers, resulting in a transparent gel that mimics the optical properties of human vitreous humor. A low concentration of metal shavings has been stirred in the gel to simulate vitreous opacities.

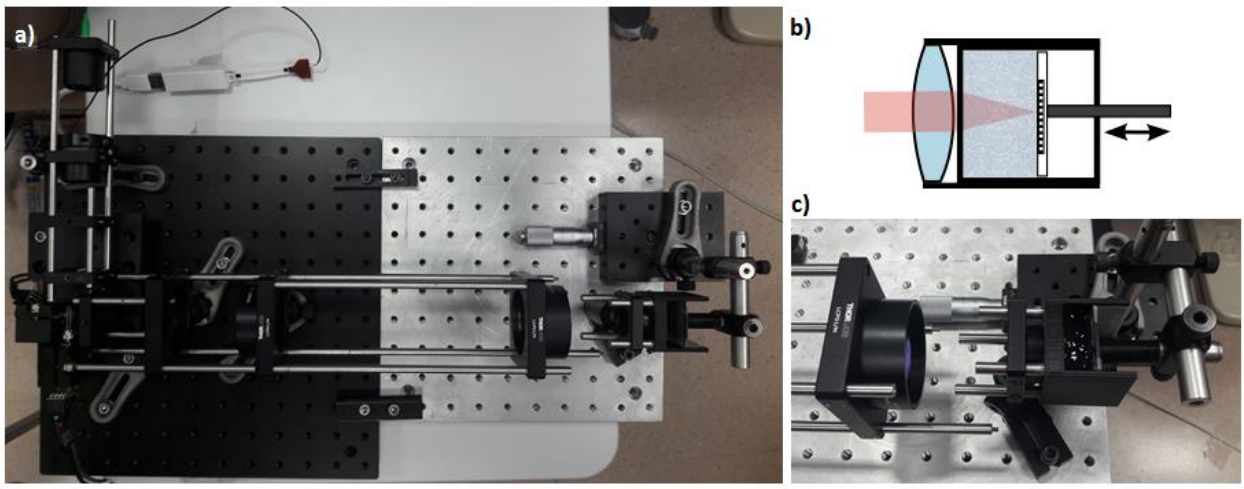

Figure 5. (a) Laboratory prototype of the vitreous imaging optical interface. (b) Scheme of an eye model prototype with a chamber to place artificial vitreous. (c) The custom eye model was 3D printed. It consists in a biconvex lens, a receptacle where the artificial vitreous humor can be placed and a movable printed calibrated target.

The example of ETL operation in SS-OCT instrument is demonstrated in Fig. 6. The ETL was driven at the frequency of 1 Hz. We acquired repeated B-scans at the position to show the impact of focus tuning on the OCT image. The scan protocol included 50 B-scans, each consisting of 1000 A-scans so that the entire scan takes a period of ETL tuning.

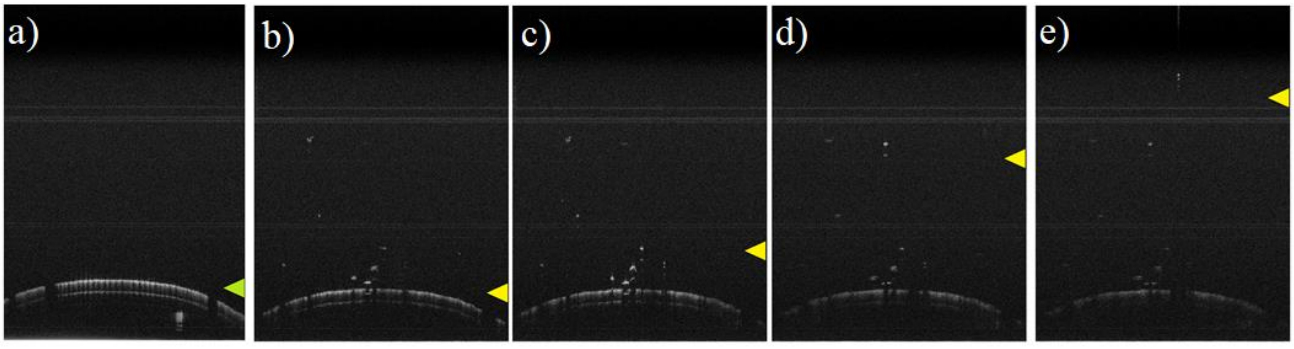

Figure 6. Preliminary demonstration of the system performance utilizing the custom developed eye model. (a) Imaging with transparent artificial vitreous. (b) Imaging of the artificial vitreous with opacities. (c)-(e) Focus tuning allows to enhance the visualization of artificial vitreous opacities at different depths.

Figure 6a illustrates the OCT image of the calibrated target through transparent artificial vitreous and the focus placed at the artificial eye retinal plane. Figure 6b shows the OCT image of the target with the focal plane at the retina through artificial vitreous with a low concentration of opacities. It can be observed that in the same conditions, the calibrated target looks distorted, the overall signal intensity has dropped and the contrast of the printed calibrated pattern has decreased considerably, caused as expected by the introduction of scatterers. Note that the artificial retina used in the experiment consisted on a plane surface, instead of curved. The longer optical path lengths at positions away from the center cause the concave appearance of the artificial retina in the images.

Figs. 6c-e illustrate the effect of ETL tuning of the focus from the retinal plane towards the lens in three consecutive focus positions. As the focal plane shifts away from the artificial retina, the collection of photons backscattered at different depths of the vitreous is enhanced, yielding the visualization of structures that were not visible otherwise. Albeit highly defocused, the retinal plane is still visible for the maximum ETL power, when the focal plane is at the farthest position.

Wrapping up the results, it has been observed that focus tuning allows highlighting opacities at different depths of the artificial vitreous. A conventional sample arm based on Gaussian optics would require a considerably loosely focused beam to achieve such long depth of focus, and consequently, very poor lateral resolution. That could jeopardize the observation of microstructures in the vitreous. The use of ETL technology in the sample arm permits to image through the whole artificial vitreous by keeping good lateral resolution without the need to draw upon more complex illumination and collection modes schemes.

4. CONCLUSIONS

We have designed a sample arm specifically dedicated for vitreous imaging, providing a FOV of 45º in the retina and allowing to switch the focal plane from retina to an extent of about 10 mm towards the crystalline lens, covering a large portion of the vitreous with good optical quality. This sample arm can be easily attached to a previously developed extended depth SS-OCT system.

Preliminary results show that the designed system allows for enhanced visualization of simulated opacities at different depths within artificial vitreous in an eye model.

In future works, the clinical potentiality of the system will be further explored. The designed interface will be used to image healthy eyes and patients suffering from vitreous related symptomatology.

ACKNOWLEDGEMENTS

The study is supported by the by the European fund within the Smart Growth Operational Programme 2014–2020 (TEAM Programme; #POIR.04.04.00-00-5C9B/17-00), by the European Research Council SEECAT grant (#ERC-2013-AdG-339228), by the by the Secretaría de Estado de Investigación, Desarrollo e Innovación (#FIS2013-41237-R) and by the European Union's Horizon 2020 research and innovation programme through the project Advanced Biomedical Optical Imaging and Data Analysis (BE-OPTICAL) Marie Skłodowska-Curie grant agreement No. 675512.

REFERENCES

1 Artal, P. Optics of the eye and its impact in vision: a tutorial. *Adv. Opt. Photon.* **6**, 340-367, (2014)
2 Grulkowski, I. *et al.* Volumetric macro- and micro-scale assessment of crystalline lens opacities in cataract patients using long-depth-range swept source optical coherence tomography. *Biomed. Opt. Express* **9**, 3821-3833, (2018).
3 de Castro, A. *et al.* Three-Dimensional Cataract Crystalline Lens Imaging With Swept-Source Optical Coherence Tomography. *Invest. Ophthalmol. Vis. Sci.* **59**, 897-903, (2018).
4 Coupland, S. E. The pathologist's perspective on vitreous opacities. *Eye* **22**, 1318-1329, (2008).
5 Sebag, J. *Vitreous in Health and Disease* (Springer, 2014).

6 Garcia, G. A. *et al.* Degradation of Contrast Sensitivity Function Following Posterior Vitreous Detachment. *Am. J. Ophthalmol.* **172**, 7-12, (2016).
7 Mamou, J. *et al.* Ultrasound-Based Quantification of Vitreous Floaters Correlates with Contrast Sensitivity and Quality of Life. *Invest. Ophthalmol. Vis. Sci.* **56**, 1611-1617, (2015).
8 Milston, R., Madigan, M. C. & Sebag, J. Vitreous floaters: Etiology, diagnostics, and management. *Surv. Ophthalmol.* **61**, 211-227, (2016).
9 Sebag, J. Imaging vitreous. *Eye* **16**, 429-439, (2002).
10 Sebag, J. Seeing the invisible: the challenge of imaging vitreous. *J. Biomed. Opt.* **9**, 38-46, (2004).
11 Grulkowski, I. in *Handbook of Visual Optics, Volume Two: Instrumentation and Vision* (ed. Pablo Artal) (CRC Press - Taylor & Francis Group, 2016).
12 Liu, J. J. *et al.* Enhanced Vitreous Imaging in Healthy Eyes Using Swept Source Optical Coherence Tomography. *PLoS One* **9**, e102950, (2014).
13 Spaide, R. F. Visualization of the Posterior Vitreous With Dynamic Focusing and Windowed Averaging Swept Source Optical Coherence Tomography. *Am. J. Ophthalmol.* **158**, 1267-1274, (2014).
14 Uji, A. & Yoshimura, N. Microarchitecture of the Vitreous Body: A High-Resolution Optical Coherence Tomography Study. *Am. J. Ophthalmol.* **168**, 24-30, (2016).
15 Takahashi, A., Nagaoka, T. & Yoshida, A. Enhanced vitreous imaging optical coherence tomography in primary macular holes. *Int. Ophthalmol.* **36**, 355-363, (2016).
16 Grulkowski, I. *et al.* Swept source optical coherence tomography and tunable lens technology for comprehensive imaging and biometry of the whole eye. *Optica* **5**, 52-59, (2018).
17 Kolb, J.P. *et al.* Ultra-widefield retinal MHz-OCT imaging up to 100 degrees viewing angle, *Biomed. Opt. Express* **6**, 1534-1552, (2015).